Electronic structure and bonding in metal phthalocyanines, Metal=Fe, Co, Ni, Cu, Zn, Mg

Meng-Sheng Liao and Steve Scheiner[a)]
Department of Chemistry and Biochemistry, Utah State University, Logan, Utah 84322-0300

(Received 28 December 2000; accepted 2 March 2001)

Electronic structure and bonding in metal phthalocyanines (Metal=Fe, Co, Ni, Cu, Zn, Mg) is investigated in detail using a density functional method. The metal atoms are strongly bound to the phthalocyanine ring in each case, by as much as 10 eV. The calculated orbital energy levels and relative total energies of these D_{4h} structures indicate that Fe and Co phthalocyanines have $^3A_{2g}$ and ^2E_g ground states, respectively, but that these states are changed upon interaction with strong-field axial ligands. The valence electronic structures of Fe and Co phthalocyanines differ significantly from those of the others. The HOMOs in Fe, Co, and Cu phthalocyanine are metal $3d$-like, whereas in Ni and Zn phthalocyanines, the HOMO is localized on the phthalocyanine ring. The first ionization removes an electron from the phthalocyanine a_{1u} orbital in all cases, with very little sensitivity of the ionization energy to the identity of the metal. Whereas the first reduction in Fe and Co phthalocyanine occurs at the metal, it is the phthalocyanine that is reduced upon addition of an electron to the other systems. Fe, Ni, and Cu phthalocyanines have smaller HOMO–LUMO separations than do Zn and Co phthalocyanine. There is very little variation in atomic charges within the phthalocyanine from one metal to the next. © *2001 American Institute of Physics.*
[DOI: 10.1063/1.1367374]

I. INTRODUCTION

Metal phthalocyanines (MPc) are interesting species that have been considered for numerous applications in industry.[1,2] The similarity in structure between phthalocyanine and the biological molecules chlorophyll and haemoglobin adds to their interest, and a huge number of different MPcs have been produced[3] over the years.[4] As a class of macrocyclic planar aromatic compounds, MPcs show special physical and chemical properties, and there have been numerous experimental studies of their optical, magnetic, and electric properties. The interpretation of the electronic spectra of MPcs has been the subject of theoretical investigations.[2,5–13] The early calculations[5–10] made use of semiempirical methods which are of questionable accuracy. More recent high-level calculations[2,12,13] were concerned mainly with the electronic spectra of metal-free phthalocyanine (H_2Pc). Kutzler and Ellis[11] reported a discrete variational X_α(DV–X_α) calculation on NiPc, focusing mainly on the band structure. More recently, Day *et al.*[14] used DFT, HF, and PM3 calculations on CuPc, SnPc, and PbPc to determine their equilibrium structures. This study also calculated vibrational and electronic spectra for H_2Pc. Piet *et al.*[15] estimated ionization potentials of ZnPc via semiempirical AM1 and PM3 methods.

The main features of the electronic structure of closed-shell MPcs (MgPc, ^{6}NiPc[11]) have been satisfactorily accounted for. However, much less is known about other MPc species, especially those with an open shell.[16] Phthalocyanines containing certain transition metals (e.g., Cr, Mn, Fe, Co) have more complex electronic structures because the open $(n-1)d$ shells may result in a number of energetically close-lying electronic states. The spectra of these compounds contain extra features arising from charge transfer transitions.[17,18] A detailed understanding of the electronic structure of these species has hence been elusive.

The large size and complexity of MPc ($C_{32}H_{18}N_8M$) makes it difficult to use standard *ab initio* methods.[16,19] Fortunately, the refinement of density-functional (DF) methods in recent years has made them a suitable, and sometimes preferable, alternative to *ab initio* approaches. The DF approach has now, with the inclusion of nonlocal exchange and correlation corrections, become a method reliable enough to be of genuine relevance in chemistry.[20] Using a recently developed DF method, a comparative and systematic study of a series of first-row transition-metal phthalocyanines (tMPc) is carried out here. Five tMPcs are chosen, FePc, CoPc, NiPc, CuPc, ZnPc, which cover the series of $3d^5$–$3d^{10}$ complexes. For the sake of comparison between transition and main-group metals, the MgPc system, where the central metal lacks d electrons, was also included. MPcs can be reduced chemically or electrochemically to yield a series of negative ions $[MPc]^{x-}$ ($x=1,2,3,4$),[21] which correspond to successive one electron addition to MPc; oxidation of MPc will produce positive $[MPc]^+$ ions.[22] Calculations were thus extended to include positive and negative MPc ions, which should provide additional information about the metal-Pc bonding.

The present work has a number of aims. The first goal is an elucidation of the electronic structure of the MPcs and their ions. The electronic configuration for FePc is somewhat controversial. A $^3B_{2g}$ ground state was originally suggested on the basis of single crystal anisotropy measurements,[23] but

a)Author to whom correspondence should be addressed; electronic mail: scheiner@cc.usu.edu

later magnetic circular dichroism spectra showed that the ground state is in fact $^3A_{2g}$.[24] In contrast, addition of a strongly coordinating axial ligand makes the species diamagnetic (closed-shell, $^1A_{1g}$).[22,24] The ground states of CoPc may be dependent upon the strength of binding to the ligand.[25] The ground state configuration of the reduced species for FePc, CoPc, and CuPc remain in doubt.[21] There is also a question concerning the nature of the oxidized species, i.e., whether it is the metal or ligand that is oxidized.[18,22]

A second aim is an exploration of the relation between calculated properties and experimental phenomena. The tMPcs (M=Fe, Co, Ni, Cu, Zn) in thin film[26] exhibit interesting redox properties that were found to correlate well with the electrochromic behaviors of the tMPcs. The authors rationalized their observed pattern in terms of decreasing electronegativity (EN) from Ni to Fe,[27] and it was argued that a central metal with higher EN could more strongly lower the electron density of the Pc ring, and consequently make the Pc more difficult to oxidize. This concept is explored by computing ionization potentials (IPs) and other properties of the various MPcs, which should be, according to the argument, a dominant factor in the oxidation potentials of the MPcs. Further, calculated IPs for outer valence MOs are useful for interpretation of experimental photoelectron spectra (PES). Because of the complex electronic structure due to a large number of MOs, the character of the MO responsible for each band in the PES of various MPcs has not been fully elucidated.[28] A last objective of this work is a theoretical discussion of several optical transitions of MPcs and their ions which have attracted the interest of both experimentalists[17,18,21,24] and theoreticians.[5–14]

II. COMPUTATIONAL METHOD

The calculations made use of the Amsterdam density-functional (ADF) program developed by Baerends *et al.*[29] and extended to the quasirelativistic method by Ziegler *et al.*[30] In this set of programs, each one-electron molecular orbital (MO) is expressed as a linear combination of atomic-centered Slater-type orbitals (STOs). The specified core electrons are described in the frozen-core approximation. Integrals are computed by three-dimensional numerical integration. The bond energy is evaluated by the so-called ''transition-state method,'' [31] an important advantage of the ADF program package.

In this work, the density functional used was based on the Vosko–Wilk–Nusair (VWN) local spin-density potential[32] plus Becke's gradient correction for exchange[33] and Perdew's gradient correction for correlation.[34] In the quasirelativistic method (one-component approach), spin–orbit (SO) coupling is not taken into account; however, the *d*-shell SO splitting in the first-row transition-metal systems is expected to be small. For the open-shell states, the unrestricted Hartree–Fock (UHF) spin-density functional approach was used.

The STO basis used is of triple-ζ quality for all atoms and relatively small core definition ([Ne] for transition metal; [He] for Mg) were used for the metal; the valence set on the metals includes $(n-1)s$ and $(n-1)p$ shells. In addition, one polarization function of $4p$ type was added to the transition metals, and two polarization functions of $3p$ and $3d$ type for Mg. For C and N, $2s$ and $2p$ were considered as valence shells and one $3d$ polarization function was added. For H, $1s$ was taken as valence shell and one $2p$ polarization was added.

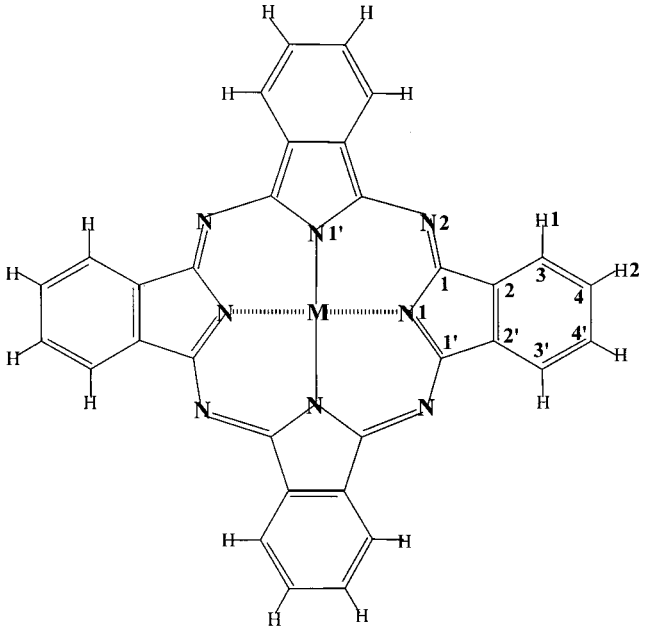

FIG. 1. Atomic numbering scheme of metal phthalocyanines.

III. RESULTS AND DISCUSSION

A. Structures

Raman spectroscopic data[35] indicate that the overall symmetry of MPc (in solution) is D_{4h}. The molecular structure of MPc is illustrated in Fig. 1 wherein the central metal (M) is coordinated to four N atoms. Full geometry optimization of each MPc under D_{2h} symmetry constraints leads to structures that are very close to the expected D_{4h} symmetry: the M–N1 and M–N1′ distances differ by less than 0.01Å. The optimized bond lengths and angles for the various MPcs are collected in Table I along with their experimental correlates. As evident in the first row, the metal–nitrogen distances in FePc, CoPc, and NiPc are similar to one another (1.92 Å), notably shorter than in CuPc (1.98 Å), or in ZnPc and MgPc, which are in turn about 0.03 Å longer still. Regarding the N1–C1 bond length within the Pc ring, FePc has the longest such bond, followed by Co and Ni, and then by the Cu, Zn, Mg group. The C1–N2 bond length, more distant from the metal, is less dependent upon the nature of the latter; even less sensitivity is observed in the other aspects of the Pc geometry.

Detailed experimental structures in the crystalline state[36–41] are reported in the indicated rows of Table I, and are consistent with the calculations. (The crystal structure of NiPc was determined more than 50 years ago,[38] and the values for the bond lengths and angles are questionable.) Electron diffraction structures are available for ZnPc and MgPc which permit a comparison between gas phase[42] and crystal, which are in overall agreement. The transition from crystal

TABLE I. Calculated structural parameters (bond length R in Å, bond angle θ in deg); atom labels from Fig. 1. Experimental data[a] reported for comparison.

		FePc	CoPc	NiPc	CuPc	ZnPc	MgPc
R_{M-N1}	Calc.	1.918	1.923	1.923	1.976	2.012, 1.955[c]	2.008, 2.008[c]
	Expt.	1.927	1.912	(1.83)[b]	1.935	1.980, 1.954[d]	2.058, 1.990[d]
R_{N1-C1}	Calc.	1.391	1.385	1.384	1.377	1.376, 1.372	1.377, 1.372
	Expt.	1.378	1.381	(1.38)	1.366	1.369, 1.374	1.366, 1.386
R_{C1-N2}	Calc.	1.322	1.322	1.320	1.328	1.334	1.335
	Expt.	1.322	1.317	(1.38)	1.328	1.331	1.332
R_{C1-C2}	Calc.	1.450	1.458	1.455	1.460	1.464, 1.461	1.465, 1.462
	Expt.	1.450	1.459	(1.46)	1.453	1.455, 1.420	1.460, 1.411
$R_{C2-C2'}$	Calc.	1.408	1.403	1.403	1.409	1.414, 1.411	1.415, 1.413
	Expt.	1.392	1.400	(1.38)	1.400	1.400, 1.550	1.399, 1.468
R_{C2-C3}	Calc.	1.399	1.396	1.397	1.397	1.396, 1.399	1.395, 1.395
	Expt.	1.395	1.394	(1.39)	1.388	1.393, 1.370	1.387, 1.400
R_{C3-C4}	Calc.	1.394	1.399	1.396	1.396	1.397, 1.399	1.397, 1.394
	Expt.	1.390	1.401		1.377	1.391, 1.369	1.380, 1.399
$R_{C4-C4'}$	Calc.	1.412	1.407	1.410	1.409	1.408, 1.399	1.406, 1.408
	Expt.	1.394	1.405		1.400	1.396, 1.383	1.395, 1.412
R_{C-H}	Calc.	1.090	1.090	1.090	1.090	1.090, 1.086	1.090, 1.086
	Expt.		1.08			1.122	1.121
$\theta_{C1-N1-C1'}$	Calc.	106.7	107.0	107.2	109.1	110.0, 109.6	109.7, 109.9
	Expt.	107.2	107.1	(99)	107.3	109.1, 106.9	108.4, 109.5
$\theta_{N2-C1-N1}$	Calc.	127.6	127.8	128.0	128.1	127.9, 127.6	127.5, 127.5
	Expt.	127.9	127.9	(126)	127.6	125.4, 125.7	127.7, 125.9
$\theta_{N1-C1-C2}$	Calc.	110.1	110.0	110.0	108.8	108.3, 108.7	108.6, 108.4
	Expt.	110.0	109.7	(115)	110.4	108.8, 113.0	109.6, 108.9

[a]X-ray diffraction data: FePc, Ref. 36; CoPc, Ref. 37; NiPc, Ref. 38; CuPc, Ref. 39; ZnPc, Ref. 40; MgPc, Ref. 41.
[b]Values in parentheses are questionable.
[c]Calculated values in this column are DFT (B3LYP/6-31G*) results from Ref. 42.
[d]Experimental values in this column refer to gas-phase electron diffraction data from Ref. 42.

to gas phase appears to shorten the M–N and C1–C2 bonds while simultaneously lengthening N1–C1, and C2–C2′ even more so. Theoretical results for the structural parameters of ZnPc and MgPc from other authors[42] are also listed in Table I for comparison. The geometries from those calculations are very similar to our own. Geometry optimizations of the $[MPc]^+$ and $[MPc]^{x-}$ ions lead to structures that are relatively unaffected by ionization, indicating that the molecular geometry of MPc is rather rigid.

One measure of the importance of geometry optimization can be gleaned from Table II which reports the difference in energy between the fully optimized charged species indicated, and the same species held to the geometry of the neutral MPc. These differences tend to lie in the neighborhood of 0.02–0.03 eV for the singly charged ions, but increase progressively for the more highly charged species. It may also be noted that the reoptimization of the ions alters the M–N distances by 0.01 Å or less in most cases.

B. Electronic structures of MPc, $[MPc]^+$, and $[MPc]^{x-}$ ($x=1,2,3,4$)

Figure 2 illustrates the energies of the upper occupied and lower vacant MOs for the ground states of the six uncharged MPcs. The orbitals are labeled according to the irreducible representation of D_{4h}. Under this point group, the five metal d orbitals transform as $a_{1g}(d_{z2})$, $b_{1g}(d_{x2-y2})$, $e_g(d_{zx},d_{yz})$, and $b_{2g}(d_{xy})$. Taking the molecule to lie in the xy plane, the d_{xz},d_{yz} orbitals have π character and the rest may be considered of σ type. The M–3d populations of some MOs are reported in parentheses, so as to assist in interpreting the metal contribution to each. Table III lists the

TABLE II. Comparison of total energies (E, eV) of the [MPc] ions calculated at their optimized geometry (R^{op}, Å), and at the geometry of neutral MPc (R^{fix}, Å).

	$[FePc]^+$	$[FePc]^-$	$[FePc]^{2-}$	$[FePc]^{3-}$	$[FePc]^{4-}$	
$E(R^{op})-E(R^{fix})$	−0.03	−0.05	−0.06	−0.15	−0.27	
$R^{op}_{Fe-N}-R^{fix}_{Fe-N}$	−0.01	0.00	−0.01	0.01	0.02	
	$[CoPc]^+$	$[CoPc]^-$	$[CoPc]^{2-}$	$[CuPc]^+$	$[CuPc]^-$	$[CuPc]^{2-}$
$E(R^{op})-E(R^{fix})$	−0.03	−0.03	−0.07	−0.02	−0.02	−0.10
$R^{op}_{M-N}-R^{fix}_{M-N}$	−0.01	−0.01	0.00	−0.02	0.00	0.01

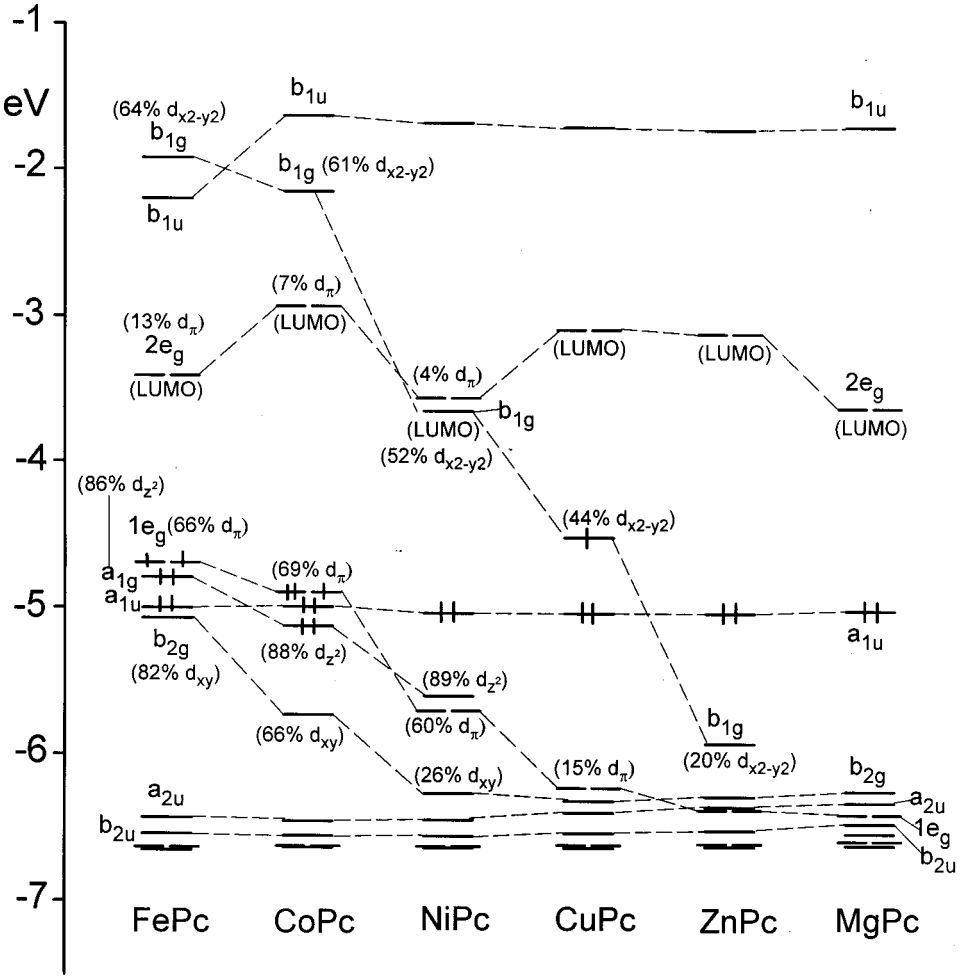

FIG. 2. Orbital energy levels for the outer orbitals in MPc.

calculated relative energies of different electronic configurations of FePc, CoPc, and CuPc, as well as a number of their ions. The calculated energy gaps between the HOMO and LUMO of the neutral and ionic states are displayed in Table IV.

1. FePc

The ground state corresponds to the electronic configuration $[\cdots](b_{2g})^2(a_{1u})^2(a_{1g})^2(1e_g)^2$, which yields a $^3A_{2g}$ state. The $1e_g$ and a_{1g} orbitals are located predominantly on the metal, with a high degree of Fe$-3d$ character; $a_{1u}(\pi)$ and $2e_g(\pi^*)$ are the HOMO and LUMO, respectively, of the Pc ring. The LUMO shows only a small amount of M$-3d_\pi$ participation: 13% for FePc, and less for the other metals, although its energy is sensitive to the nature of the metal. The a_{1u} is purely associated with Pc, and its energy is unaffected by metal substitution. The empty b_{1g} orbital, which is largely composed of Fe's d_{x2-y2}, is high, above the b_{1u} orbital which is associated with the Pc. Since the a_{1g}, a_{1u}, and b_{2g} are located near the HOMO level, excitation of an electron from any of these orbitals to the partially occupied $1e_g$ HOMO does not require much energy. The second lowest state is ^3E_g, only 0.07 eV higher than $^3A_2$, wherein one of the a_{1g} electrons has been transferred to $1e_g$. The energy of $^3B_{2g}$ also comes quite close to that of $^3A_{2g}$, combining the latter transfer along with an excitation from b_{2g} to $1e_g$. The lowest closed-shell configuration, $(b_{2g})^2(a_{1u})^2(a_{1g})^0(1e_g)^4$, lies higher than the ground state by 1.4 eV.

The ground state of cationic $[\mathrm{FePc}]^+$ corresponds to $^4A_{2u}[(b_{2g})^2(a_{1g})^2(a_{1u})^1(1e_g)^2]$. Comparison with the neutral indicates that the one-electron oxidation in FePc takes place from the a_{1u} orbital of the Pc ring and not from the metal d orbital, even though the a_{1g} and $1e_g$ orbitals lie above a_{1u}. The first and second reductions of FePc to yield $[\mathrm{FePc}]^-$ and $[\mathrm{FePc}]^{2-}$ involve electron addition to metal d orbitals, in agreement with ESR observations.[22] $[\mathrm{FePc}]^-$ has a ground state of $^2A_{1g}[(1e_g)^4(b_{2g})^2(a_{1g})^1]$: when the added electron goes into $1e_g$, there is rearrangement of the d electrons and the a_{1g} and $1e_g$ orbitals switch their ordering. The calculated ground state for $[\mathrm{FePc}]^-$ is also consistent with the ESR results which indicate that $[\mathrm{FePc}]^-$ is a low-spin d^7 complex with a d_{z2}^1 ground state.[22] It may be noted from the last column of Table III that it is only the third additional electron, i.e., in $[\mathrm{FePc}]^{3-}$, that is added to the Pc. For the third and fourth reductions, electrons enter the LUMO $2e_g$ on the Pc ring, as the metal a_{1g} is completely filled. IR/vis spectra[21] on $[\mathrm{FePc}]^{3-}$ were interpreted in terms of a $^4A_{2g}[(a_{1g})^1(2e_g)^2]$ ground state, which is calculated to lie within 0.07 eV of ^2E_g. A $^3E_g[(a_{1g})^1(2e_g)^3]$ ground state for $[\mathrm{FePc}]^{4-}$ was assumed by experiment,[21] which lies $\sim$0.5 eV above the $^3A_{2g}$ state according to the calculations.

TABLE III. Calculated relative energies (eV) for various electronic configurations.

	Configuration	Term	E^{relative}	n_M, n_{Pc}[a]
FePc	$(b_{2g})^2(a_{1u})^2(a_{1g})^2(1e_g)^2$	$^3A_{2g}$	0	
	$(b_{2g})^2(a_{1u})^2(a_{1g})^1(1e_g)^3$	^3E_g	0.07	
	$(b_{2g})^1(a_{1u})^2(a_{1g})^1(1e_g)^4$	$^3B_{2g}$	0.10	
	$(b_{2g})^1(a_{1u})^2(a_{1g})^2(1e_g)^3$	^3E_g	0.57	
	$(b_{2g})^2(a_{1u})^1(a_{1g})^1(1e_g)^4$	$^3A_{1u}$	0.67	
	$(b_{2g})^2(a_{1u})^2(a_{1g})^0(1e_g)^4$	$^1A_{1g}$	1.42	
	$(b_{2g})^2(a_{1u})^0(a_{1g})^2(1e_g)^4$	$^1A_{1g}$	2.21	
	$(b_{2g})^0(a_{1u})^2(a_{1g})^2(1e_g)^4$	$^1A_{1g}$	2.72	
$[FePc]^+$	$(b_{2g})^2(a_{1g})^2(a_{1u})^1(1e_g)^2$	$^4A_{2u}$	0	
	$(b_{2g})^2(a_{1g})^1(a_{1u})^2(1e_g)^2$	$^4A_{2g}$	0.05	
	$(b_{2g})^1(a_{1g})^2(a_{1u})^2(1e_g)^2$	$^4B_{1g}$	0.21	
	$(b_{2g})^2(a_{1g})^2(a_{1u})^2(1e_g)^1$	^2E_g	0.88	
$[FePc]^-$	$(a_{1u})^2(1e_g)^4(b_{2g})^2(a_{1g})^1$	$^2A_{1g}$	0	1, 0
	$(a_{1u})^2(1e_g)^3(b_{2g})^2(a_{1g})^2$	^2E_g	0.37	
	$(a_{1u})^2(1e_g)^4(b_{2g})^1(a_{1g})^2$	$^2B_{2g}$	0.61	
	$(a_{1u})^2(1e_g)^2(b_{2g})^2(a_{1g})^2(2e_g)^1$	^4E_g	0.81	
$[FePc]^{2-}$	$(b_{1g})^2(a_{1g})^2$	$^1A_{1g}$	0	2, 0
	$(b_{1g})^2(a_{1g})^1(2e_g)^1$	^3E_g	0.12	
$[FePc]^{3-}$	$(a_{1g})^2(2e_g)^1$	^2E_g	0	2, 1
	$(a_{1g})^1(2e_g)^2$	$^4A_{2g}$	0.07	
$[FePc]^{4-}$	$(a_{1g})^2(2e_g)^2$	$^3A_{2g}$	0	2, 2
	$(a_{1g})^1(2e_g)^3$	^3E_g	0.46	
CoPc	$(a_{1g})^2(a_{1u})^2(1e_g)^3$	^2E_g	0	
	$(a_{1g})^1(a_{1u})^2(1e_g)^4$	$^2A_{1g}$	0.11	
	$(a_{1g})^2(a_{1u})^1(1e_g)^4$	$^2A_{1u}$	0.31	
$[CoPc]^+$	$(a_{1g})^2(a_{1u})^1(1e_g)^3$	^3E_u	0	
	$(a_{1g})^2(a_{1u})^2(1e_g)^2$	$^3A_{2g}$	0.19	
	$(a_{1g})^1(a_{1u})^2(1e_g)^3$	^3E_g	0.54	
$[CoPc]^-$	$(1e_g)^4(a_{1g})^2$	$^1A_{1g}$	0	1, 0
	$(1e_g)^4(a_{1g})^1(2e_g)^1$	^3E_g	0.87	
$[CoPc]^{2-}$	$(a_{1g})^2(2e_g)^1$	^2E_g	0	1, 1
	$(a_{1g})^1(2e_g)^2$	^4E_g	0.75	
$[CoPc]^{3-}$	$(a_{1g})^2(2e_g)^2$	$^3A_{2g}$	0	1, 2
	$(a_{1g})^1(2e_g)^3$	^3E_g	0.84	
$[CoPc]^{4-}$	$(a_{1g})^2(2e_g)^3$	^2E_g	0	1, 3
	$(a_{1g})^1(2e_g)^4$	$^2A_{1g}$	0.61	
$[CuPc]^+$	$(a_{1u})^1(b_{1g})^1$	$^3B_{1u}$	0	
	$(a_{1u})^2(b_{1g})^0$	$^1A_{1g}$	0.71	
$[CuPc]^-$	$(a_{1u})^2(b_{1g})^1(2e_g)^1$	^3E_g	0	0, 1
	$(a_{1u})^2(b_{1g})^2(2e_g)^0$	$^1A_{1g}$	0.45	
$[CuPc]^{2-}$	$(a_{1u})^2(b_{1g})^1(2e_g)^2$	$^4B_{2g}$	0	0, 2
	$(a_{1u})^2(b_{1b})^2(2e_g)^1$	^2E_g	0.64	
$[CuPc]^{3-}$	$(a_{1u})^2(b_{1g})^1(2e_g)^3$	^3E_g	0	0, 3
	$(a_{1u})^2(b_{1g})^2(2e_g)^2$	$^3A_{2g}$	0.45	
$[CuPc]^{4-}$	$(a_{1u})^2(b_{1g})^1(2e_g)^4$	$^2B_{1g}$	0	0, 4
	$(a_{1u})^2(b_{1g})^2(2e_g)^3$	^2E_g	0.04	

[a]n_M and n_{Pc} refer to the number of electrons added to the metal and Pc, respectively, in the indicated anion, compared to the neutral MPc.

2. CoPc

The ^2E_g ground state of CoPc is calculated to be related to that of FePc by addition of one electron to the $1e_g$ level. The $^2A_{1g}$ state, wherein one of the a_{1g} electrons is displaced to fill $1e_g$, lies just above it, by 0.1 eV. The metal $3d_\pi$-like orbitals lie between the Pc HOMO (a_{1u}) and LUMO ($2e_g$), similar to the FePc case. Compared to FePc, the $2e_g$ LUMO in CoPc manifests less M$-d_\pi$ mixing. The gap between $a_{1g}(d_{z2})$ and $b_{2g}(d_{xy})$ is enlarged as b_{2g} is lowered. The empty b_{1g}(M$-d_{x2-y2}$) is now lower than b_{1u}. CoPc behaves very much like FePc, in that the one-electron oxidation of both occurs from the Pc a_{1u} orbital, and the first reduction step involves addition of an electron to the partially filled $1e_g$. The second reduction yields $[CoPc]^{2-}$ where one excess electron resides on the metal and one on the Pc. For the thrice reduced species, two electrons reside on Pc and one on the metal. Experimentalists[21] assigned all three electrons to the Pc $2e_g$ orbital, a point of disagreement with the calculations. $[CoPc]^{4-}$ has a ^2E_g ground state wherein the unpaired electron is situated on Pc, in agreement with ESR data.[21]

3. NiPc

The $3d$ orbitals of Ni are considerably lower in energy, when compared with Fe and Co. As a result, the occupied $3d$-like orbitals lie significantly below the Pc a_{1u} orbital, making the latter the HOMO of the system. The $3d_\pi$ participation in $2e_g$ is further diminished from M=Co to Ni. The empty $3d$-like b_{1g} orbital (d_{x2-y2}) lies just beneath $2e_g$. The one-electron oxidation occurs from the a_{1u} HOMO. In the case of reduction, the first electron is added to the $1e_g(\pi)$ orbital of Pc, leaving $b_{1g}(d_{x2-y2})$ unoccupied. Addition of electrons to $2e_g$ raises the energy of b_{1g}, placing the latter above the former. $2e_g$ and b_{1g} represent the HOMO and LUMO, respectively, in $[NiPc]^{x-}$ (see Table IV).

4. CuPc

The $3d$ orbitals continue to be lowered as one progresses from Ni to Cu. The $3d$-like b_{1g} orbital is half occupied and positioned in the gap between the Pc HOMO and LUMO. As evident in Table III, the one-electron oxidation occurs from a_{1u} although b_{1g} lies some 0.5 eV higher (ionization from b_{1g} requires 0.7 eV more than that from a_{1u}). The ground states of the $[CuPc]^{x-}$-ions have a $(b_{1g})^1(2e_g)^x$ configuration; i.e., all reduction steps correspond to deposition of electrons into the Pc $2e_g$ orbital, bypassing the lower

TABLE IV. Calculated energy gaps (eV) between HOMO and LUMO.[a]

	M=Fe	M=Co	M=Ni	M=Cu	M=Zn	M=Mg[b]
MPc	1.38($1e_g$,$2e_g$)	1.96($1e_g$,$2e_g$)	1.47(a_{1u},b_{1g})	1.42(b_{1g},$2e_g$)	1.91(a_{1u},$2e_g$)	1.38
$[MPc]^+$	1.95($1e_g$,$2e_g$)	2.10($1e_g$,$2e_g$)	1.84(a_{1u},b_{1g})	1.50(b_{1g},$2e_g$)	1.90(a_{1u},$2e_g$)	1.36
$[MPc]^-$	1.72(a_{1g},$2e_g$)	1.48(a_{1g},$2e_g$)	0.58($2e_g$,b_{1g})	1.24($2e_g$,b_{1u})	1.25($2e_g$,b_{1u})	1.26
$[MPc]^{2-}$	1.13(a_{1g},$2e_g$)	1.41($2e_g$,b_{1u})	0.71($2e_g$,b_{1g})	1.09($2e_g$,b_{1u})	1.12($2e_g$,b_{1u})	1.64
$[MPc]^{3-}$	1.03($2e_g$,b_{1u})	1.25($2e_g$,b_{1u})	0.86($2e_g$,b_{1g})	0.96($2e_g$,b_{1u})	0.98($2e_g$,b_{1u})	1.01
$[MPc]^{4-}$	0.96($2e_g$,b_{1u})	0.74($2e_g$,b_{1g})	0.89($2e_g$,b_{1g})	1.39($2e_g$,b_{1u})	0.87($2e_g$,b_{1u})	0.90

[a]Orbitals in brackets represent HOMO and LUMO, respectively.
[b]HOMO and LUMO for M=Mg are the same as for M=Zn.

TABLE V. Gross Mulliken populations and atomic charges (Q).

		M=Fe	M=Co	M=Ni	M=Cu	M=Zn	M=Mg
MPc	$3d$	6.59	7.63	8.61	9.50	10.0	0.42($3d$)
	$4s$	0.42	0.41	0.42	0.39	0.55	0.36($3s$)
	$4p$	0.29	0.37	0.48	0.46	0.81	0.45($3p$)
	Q_{M}	0.71	0.59	0.50	0.65	0.64	0.87
	Q_{N1}	−0.53	−0.50	−0.48	−0.51	−0.49	−0.57
	Q_{N2}	−0.33	−0.33	−0.33	−0.33	−0.33	−0.33
	Q_{C1}	0.32	0.32	0.32	0.32	0.32	0.33
	Q_{C2}	0.09	0.09	0.09	0.09	0.08	0.08
	Q_{C3}	0.14	0.14	0.14	0.14	0.14	0.13
	Q_{C4}	0.17	0.17	0.17	0.17	0.17	0.17
	Q_{H1}	−0.18	−0.18	−0.19	−0.18	−0.18	−0.18
	Q_{H2}	−0.18	−0.18	−0.18	−0.18	−0.18	−0.18
$[\mathrm{MPc}]^{+}$	$3d$	6.59(6.53)[a]	7.64(7.57)	8.61	9.50	10.0	0.40
	$4s$	0.40(0.30)	0.36(0.38)	0.40	0.37	0.54	0.31
	$4p$	0.27(0.35)	0.39(0.39)	0.47	0.45	0.80	0.40
	Q_{M}	0.74(0.82)	0.62(0.66)	0.52	0.68	0.65	0.90
$[\mathrm{MPc}]^{-}$	$3d$	6.70	7.73	8.62	9.50	10.0	0.40
	$4s$	0.33	0.46	0.44	0.40	0.57	0.33
	$4p$	0.31	0.34	0.48	0.47	0.81	0.42
	Q_{M}	0.67	0.48	0.47	0.63	0.62	0.85
$[\mathrm{MPc}]^{2-}$	$3d$	6.71	7.73	8.62	9.50	10.0	0.41
	$4s$	0.52	0.49	0.46	0.41	0.53	0.34
	$4p$	0.26	0.34	0.48	0.48	0.82	0.43
	Q_{M}	0.52	0.44	0.44	0.61	0.60	0.82
$[\mathrm{MPc}]^{3-}$	Q_{M}	0.45	0.39	0.41	0.58	0.59	0.80
$[\mathrm{MPc}]^{4-}$	Q_{M}	0.38	0.33	0.37	0.56	0.57	0.78

[a]The values in parentheses are those obtained when an electron is removed from M $3d$ orbital.

$b_{1g}(d_{x2-y2})$. This preference for $2e_g$ may be due to repulsion terms that are lower for addition of electrons into the more diffuse Pc orbital compared to the more localized metal d orbital.

5. ZnPc and MgPc

When M=Zn, the $3d$ subshell is filled and deep enough to form rather pure MOs. ZnPc and MgPc exhibit a large gap between the HOMO and LUMO. The positive $[\mathrm{MPc}]^{+}$ ion results from removal of an electron from the a_{1u} HOMO and all negative ions from the addition of electrons to the $2e_g$ LUMO. In short, the valence electronic structures of ZnPc and MgPc are very similar. Thus, the spectra for oxidation and reduction of ZnPc are expected to resemble closely those of MgPc, as is indeed the case according to optical studies.[21]

6. Charge distribution

The calculated gross populations of the various atomic orbitals and Mulliken atomic charges are collected in Table V. Although the metal atom has a formal charge of +2 in the neutrals, the effective atomic charge is calculated to lie between 0.5 and 0.9. This difference suggests that the bonding between M and Pc is not purely ionic, but significantly covalent. The positive charge of M decreases from Fe to Ni, as expected according to the electronegativities, but the variation is small. Whereas the low electronegativity of Zn results in a greater positive charge, the high electronegativity of Cu is not apparent in Q_{M}. The electronegativity of nitrogen leads to some accumulation of charge. N1 is more negatively charged than is N2, probably owing to the overlap of the former with the metal orbitals. While there is some sensitivity of the N1 charge to the nature of the metal, the charge distributions on N2, and the C and H atoms within the Pc system, are largely unaffected. The latter observation belies an earlier presumption[26a] that the different behavior of the various MPcs is moderated by the electron density on the periphery of the Pc system, which is in turn induced by changes in the metal's electronegativity.

Regarding the individual atomic orbitals, both $4s$ and $4p$ subshells of the metal are significantly populated, mainly due to σ donation from Pc. The $4p$ population increases from Fe to Zn, although the values for Ni and Cu are very similar. The Zn $4p$ value exceeds 0.8, indicating that polarization effects are especially important for Zn–Pc bonding. The gross M $3d$ population in MPc varies by 3.4 in going across from FePc to ZnPc; much smaller changes occur in the M $4s$ population.

Turning to the ions, for $[\mathrm{MPc}]^{+}$, where an electron is ionized from the Pc a_{1u}, the charges on M are decreased by only 0.03 or less; the density loss is restricted almost entirely to the Pc ring. For $[\mathrm{FePc}]^{+}$ and $[\mathrm{CoPc}]^{+}$, the M–AO populations and charge distributions were also examined after removal of an electron from a $3d$-like orbital. In each case, the decrease in the M–$3d$ population is about 0.06, indicating a certain amount of charge flows from the Pc ring to M, as

TABLE VI. Comparison of calculated properties[a] for D_{4h} (open-shell) and D_{2h} (closed-shell) configurations of $[MPc]^{2-}$ for M=Zn and Mg.

		R_{M-N1}	R_{M-N2}	$E^{relative}$	HOMO	Q_M
$[ZnPc]^{2-}$	D_{4h}	2.02	2.02	0	$(2e_g)^2$	0.60
	D_{2h}	2.01	2.04	−0.06	$(b_{2g})^2$	0.61
$[MgPc]^{2-}$	D_{4h}	2.02	2.02	0	$(2e_g)^2$	0.82
	D_{2h}	2.01	2.03	−0.07	$(b_{2g})^2$	0.84

[a]Bond length R in Å, relative energy E in eV, charge distribution on metal Q_M in e.

indicated by the entries in parentheses in Table V. The resulting net increase of positive charge on M is less than 0.1, as compared to the electron removal from a_{1u}. As in the case of the cations, the charge assigned to the metal in the anionic $[MPc]^-$ is also quite similar to that in the neutral, especially for M=Ni, Cu, Zn, and Mg, where the added electron goes into the Pc orbital. The charges in $[FePc]^-$ and $[CoPc]^-$ are 0.04 and 0.11 less positive than in FePc and CoPc, respectively. Whereas the first reduction of FePc and CoPc is believed to occur at the metal, the gross $3d$ population as well as the atomic charge on M are changed by only a little. It is concluded that the addition of an electron to the M−$3d$ orbital is accompanied by electron movement from M to Pc. The Pc macrocycle plays the role of an electron buffer in the metal oxidation and reduction. The last few rows of Table V show that further reductions add only small increments of atomic charge to the metal.

7. The role of Jahn–Teller effects in $[MPc]^{2-}$

The ground state of the $[MPc]^{2-}$ ion under D_{4h} symmetry, for M=Ni, Zn, and Mg, has an open-shell configuration $(a_{1u})^2(2e_g)^2$, which should represent a triplet. However, experimental studies[6,18] indicated a diamagnetic species (spin-paired diion). This discrepancy was explained by a pseudo-Jahn–Teller (JT) effect that stabilizes $^1A_{1g}$ with respect to $^3A_{2g}$. The energetics of the distortion process of $[MPc]^{2-}$ from D_{4h} to D_{2h} were thus investigated here, with M=Zn and Mg as examples. In reduced D_{2h} symmetry, the $2e_g$ level is split into b_{2g} and b_{3g}. A geometry optimization was carried out under D_{2h} molecular symmetry and with $(b_{2g})^2$ occupation (closed-shell configuration). The calculated properties of the D_{4h} and D_{2h} geometries are compared in Table VI, and the orbital energy levels illustrated in Fig. 3. When the constraints of D_{4h} symmetry are relaxed to D_{2h}, the M–N1 distance becomes 0.02–0.03 Å shorter than M–N2. The smallness of this distortion may be ascribed to the rigidity of the molecule. Relative to $2e_g$, the energy level of b_{2g} is lowered by the distortion by only ~0.1 eV, accompanied by a lowering of the total molecular energy by a comparable amount. Therefore, for free $[MPc]^{2-}$, the D_{2h} structure is favored energetically over D_{4h}, but only to a small degree. It is suggested that for $[MPc]^{2-}$ in solution, other factors arising from bonding interactions with cations may play a more dominant role in causing the distortion.

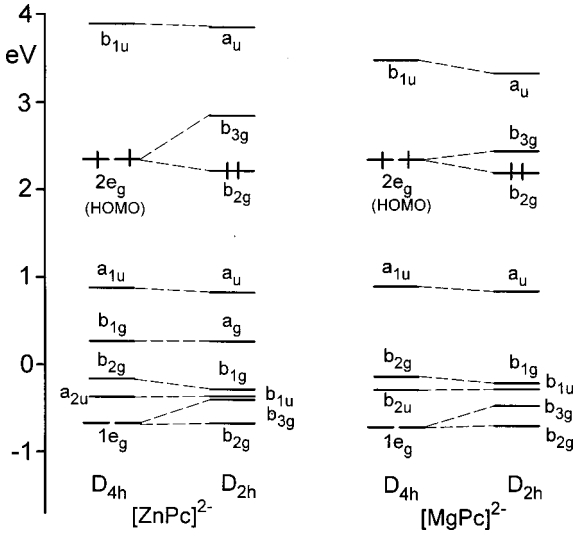

FIG. 3. Orbital energy level diagrams for D_{4h} and D_{2h} configurations of $[MPc]^{2-}$ for M=Zn and Mg.

C. M–Pc binding energies and electron affinities

Further insights into the bonding in MPc and $[MPc]^{x-}$ can be gleaned from Table VII which lists the calculated M–Pc binding energies (E_{bind}) and electron affinities (EA) of $[MPc]^{x-}$ ($x=0,1,2,3$). These quantities are defined in terms of the energies of the various species as follows:

$$E_{bind}=E(MPc)-\{E(M)+E(Pc)\},$$

$$EA=E(MPc^{(x+1)-})-E(MPc^{x-}).$$

The calculated binding energies vary between 5.7 eV for ZnPc to 10.5 eV for CoPc. These large interactions between the metal and the Pc are consistent with the high thermal and chemical stability of MPc. E_{bind} is quite sensitive to the nature of the metal, and varies in the order Co>Fe~Ni>Cu>Zn, with a large gap separating the first three from the last two. The trend in the binding energies parallels the M–N1 bond lengths in that large E_{bind} is associated with shorter R_{M-N1}.

The calculated electron affinities of MPc are all quite negative, exceeding 1.7 eV, which indicates a strong attraction of an electron for each MPc species. FePc and CoPc are particularly strong in this regard, and CuPc the weakest. This observation can be understood on the basis of the electronic structures of the $[MPc]^-$ ions. The added electron in $[FePc]^-$ and $[CoPc]^-$ occupies a low-lying bonding orbital, whereas in the other $[MPc]^-$ ions, the added electron goes into a high-lying antibonding Pc $2e_g$. The progressively

TABLE VII. Calculated M–Pc binding energies (E_{bind}, eV) and electron affinities (EA, eV).

		M=Fe	M=Co	M=Ni	M=Cu	M=Zn	M=Mg
E_{bind}	MPc	−9.81	−10.49	−9.90	−6.96	−5.66	−8.14
EA	MPc	−2.92	−3.19	−2.14	−1.74	−2.23	−2.16
	$[MPc]^-$	0.84	0.95	0.80	0.27	0.74	0.68
	$[MPc]^{2-}$	3.86	3.88	3.94	3.85	3.77	3.80
	$[MPc]^{3-}$	6.72	7.02	6.69	6.64	6.61	6.57

TABLE VIII. Calculated ionization potentials (IP, eV) for several outer molecular orbitals[a] of MPc.

System	Orbital	IP			Percent character	
		ΔSCF[b]	TS[c]	Expt.[d]	M	Pc
H_2Pc	a_{1u}	6.52	6.55	6.41		
	a_{2u}	7.69	7.72			
	$1e_g$	8.00	8.02			
	b_{2g}	8.12	8.25			
FePc	a_{1u}	6.46	6.49	6.36		100 a_{1u}
	a_{1g}	6.51	6.98	6.88	86 $3d_{z2}$, 11 $4s$	
	b_{2g}	6.67	7.19		83 $3d_{xy}$	17 b_{2g}
	$1e_g$	7.34	7.81		69 $3d_{\pi}$	31 $1e_g$
	a_{2u}	7.85	7.87			100 a_{2u}
CoPc	a_{1u}	6.47	6.47	6.38		100 a_{1u}
	$1e_g$	6.66	7.07		69 $3d_{\pi}$	31 $1e_g$
	a_{1g}	7.01	7.46		88 $3d_{z2}$, 9 $4s$	
	b_{2g}	7.46	7.64		66 $3d_{xy}$	34 b_{2g}
	a_{2u}	7.88	7.89			100 a_{2u}
NiPc	a_{1u}	6.56	6.51	6.38		100 a_{1u}
	$1e_g$	7.38	7.50	7.75	60 $3d_{\pi}$	40 $1e_g$
	a_{2u}	7.88	7.88			100 a_{2u}
	b_{2g}	7.97	8.05	8.50	26 $3d_{xy}$	74 b_{2g}
	a_{1g}	8.23	8.75		89 $3d_{z2}$, 8 $4s$	
CuPc	a_{1u}	6.51	6.51	6.38		100 a_{1u}
	b_{1g}	7.22	7.23	7.45	44 $3d_{x2-y2}$	56 b_{1g}
	$1e_g$	7.71	7.77		15 $3d_{\pi}$	85 $1e_g$
	a_{2u}	7.82	7.82			100 a_{2u}
	b_{2g}	8.02	8.11		6 $3d_{xy}$	94 b_{2g}
ZnPc	a_{1u}	6.56	6.52	6.37		100 a_{1u}
	a_{2u}	7.78	7.77			100 a_{2u}
	$1e_g$	7.81	7.86			100 $1e_g$
	b_{1g}	7.95	8.05		20 $3d_{x2-y2}$	80 b_{1g}
	b_{2g}	7.98	8.10			100 b_{2g}
MgPc	a_{1u}	6.52	6.48	6.35		100 a_{1u}
	a_{2u}	7.75	7.75			100 a_{2u}
	$1e_g$	7.83	7.88			100 $1e_g$
	b_{2g}	7.94	8.07			100 b_{2g}
	a_{1g}	9.04	9.01			100 a_{1g}

[a]For the orbital labelings, see Fig. 2.
[b]From separate SCF calculations for the neutral and ionized systems.
[c]Evaluated by using Slater transition state method.
[d]Reference 44.

more positive entries for the anions in Table VII can be attributed to increasing Coulomb repulsion with each additional electron. These anions may be rather unstable unless complexed with counter-ions or polar ligands in solution.

D. Ionization potentials

The calculated ionization potentials (IP) for several outer MOs of the MPcs are presented in Table VIII. The ΔSCF method computes the IP as the difference in total energy between the neutral and ionized species. These results are compared with those obtained by the Slater transition state (TS) method.[43] The two quantities are generally quite close when the electron is excited from the Pc ring, but can differ substantially (~0.4 eV) when the electron is ionized from a metal *d*-like orbital. Experimental gas-phase photoelectron spectra[44] (PES) for H_2Pc and MPcs with definite assignment are listed in Table VIII and suggest that the TS values are slightly superior to ΔSCF.

It was shown in Sec. III B that the first oxidation of MPc to yield $[MPc]^+$ occurs from the a_{1u} orbital of the Pc ring, whether or not this orbital is in fact the HOMO. This observation is supported by the data in Table VIII which indicate that the Pc a_{1u} has the lowest IP for each of the MPcs. The first IP is calculated to be about 6.5 eV, consistent with the PES values of ~6.4 eV, listed in the third column of data in Table VIII. There is almost no variation of the IP with the metal, reaffirming the close connection of the a_{1u} orbital with the Pc ring. Indeed, eliminating the metal entirely, as in H_2Pc, leaves IP essentially unchanged. The ionization potentials of the other orbitals listed in Table VIII are generally consistent with the orbital energy diagrams of Fig. 2. For example, Table VIII confirms the progressively deepening energy of the $a_{1g}(d_z2)$ orbital as one progresses from Fe to Co to Ni, etc. But there are exceptions as well, as in the case of the $1e_g$ orbital whose ionization potential diminishes in this same progression.

TABLE IX. Calculated first, second, and third ionization potentials (eV) for M and MPc.

	1st IP	2nd IP	3rd IP		1st IP	2nd IP	3rd IP	OP in Solut./V[a]
Fe	8.02	17.05	31.34	FePc	6.46	9.57	12.44	0.19
Co	8.53	17.64	33.78	CoPc	6.47	9.51	12.78	0.77
Ni	8.32	19.77	36.09	NiPc	6.56	9.50	13.12	1.05
Cu	8.69	21.24	38.52	CuPc	6.51	9.59	13.10	0.98
Zn	9.81	19.04	40.45	ZnPc	6.56	9.55	13.41	0.68
Mg	7.71	15.30	80.62	MgPc	6.52	9.51	13.37	

[a]Experimental oxidation potential (in voltage) in solution, Ref. 26a.

It was mentioned above that the (electrochemical) oxidation potentials of the MPcs in thin film exhibit substantial variation with a change in the central metal. Similar behavior was also observed for metal porphyrins in solution.[45] According to the calculations and PES measurements, changes in the central metal exert little effect upon the ionization potential. Therefore the trend in the oxidation potentials cannot be accounted for by the IP data alone. Similarly, our calculations do not support the argument[26(a)] that the central metal changes the electronic state of the Pc ring, thereby causing a change in the oxidation potential of MPc.

On the other hand, it has been shown that the oxidation potential of MPc may be related to the third ionization potential of the metal atom.[46] To examine the relationship, we have calculated this quantity for both isolated metal atoms and MPcs. The results are reported in Table IX, together with the experimental oxidation potentials in the final column. It may be seen that the trend in the third IPs approximately parallels the oxidation potentials (except for the Zn species). Finally, the second IP corresponds to electron extraction from Pc a_{1u} in all cases, and so it is almost independent of the metal.

E. Electron transition energies

MPcs exhibit some remarkable optical properties. The conjugated π system leads to intense electronic absorption bands in the visible region, the interpretation of which has been the subject of theoretical studies.[5–14] Most of the previous calculations were limited to semiempirical levels, and were mainly devoted to closed-shell MPcs (H_2Pc, MgPc).

TABLE X. Calculated electronic transition energies[a] (eV) (experimental values[b] in parentheses).

	Ground State	$a_{1u}\rightarrow 2e_g$ (Q band)	$a_{2u}\rightarrow 2e_g$ (Soret band)	$a_{1u}\rightarrow 1e_g$; b_{1g} (L→M)[c]	$a_{2u}\rightarrow 1e_g$ (L→M)	$1e_g\rightarrow b_{1u}$ (M→L)[b]
FePc	$^3A_{2g}$	1.64 (1.89)	3.13 (3.76)	0.45; 3.80	1.92	3.04
$[FePc]^+$	$^2A_{1u}$	1.64 (1.86)	2.99 (3.81)	0.46	1.79	3.06
$[FePc]^-$	$^2A_{1g}$	1.73 (1.85)	3.24 (3.81)	2.84(M-$a_{1g}\rightarrow$L-b_{1u})		
$[FePc]^{2-}$	$^1A_{1g}$	1.93	3.32	1.76(M-$a_{1g}\rightarrow$L-b_{1u})		
$[FePc]^{3-}$	^2E_g	2.00	3.29	1.49(M-$a_{1g}\rightarrow$L-b_{1u}), 0.60(L-$2e_g\rightarrow$L-b_{1u})		
$[FePc]^{4-}$	$^1A_{1g}$	2.08	3.26	1.26(M-$a_{1g}\rightarrow$L-b_{1u}), 0.45(L-$2e_g\rightarrow$L-b_{1u})		
CoPc	^1E_g	1.56 (1.85)	3.10 (3.56)	0.16	1.66	3.43
$[CoPc]^+$	^3E_u	1.56 (1.82)	2.95 (3.37)	0.17	1.52	3.44
$[CoPc]^-$	$^1A_{1g}$	1.71 (1.79)	3.24 (3.97)	3.53(L-$a_{1u}\rightarrow$M-b_{1g})		
$[CoPc]^{2-}$	^2E_g	1.77 (1.82)	3.22 (3.89)	0.94(1.35)(L-$2e_g\rightarrow$L-b_{1u})		
$[CoPc]^{3-}$	$^1A_{1g}$	1.90 (2.43)	3.16 (3.80)	0.77(1.05)(L-$2e_g\rightarrow$L-b_{1u})		
$[CoPc]^{4-}$	^2E_g	1.87 (2.17)	3.12	0.63(1.24)(L-$2e_g\rightarrow$L-b_{1u})		
NiPc	$^1A_{1g}$	1.50 (1.85)	3.00 (3.53)	2.17(L-$a_{1u}\rightarrow$M-b_{1g})		
$[NiPc]^+$	$^2A_{1u}$	1.50	2.84	0.91(L–M-$1e_g\rightarrow$L-a_{1u})		
$[NiPc]^-$	^2E_g	1.54 (1.97)	3.09 (3.72)	1.28(1.36)(L-$2e_g\rightarrow$L-b_{1u})		
$[NiPc]^{2-}$	$^1A_{1g}$	1.65 (2.31)	3.06 (3.72)	1.13(1.36)(L-$2e_g\rightarrow$L-b_{1u})		
$[NiPc]^{3-}$	^2E_g	1.61 (2.10)	2.97 (3.72)	0.99(1.14)(L-$2e_g\rightarrow$L-b_{1u})		
CuPc	$^2B_{1g}$	1.46 (1.75)[d]	2.92 (3.7)[d]	1.57(L-$a_{1u}\rightarrow$M-b_{1g}), 2.94(L-$a_{2u}\rightarrow$M-b_{1g})		
$[CuPc]^+$	$^3B_{1u}$	1.45	2.76	1.20(L-$1e_g\rightarrow$L-a_{1u})		
$[CuPc]^-$	^3E_g	1.52	2.97	1.28(L-$2e_g\rightarrow$L-b_{1u})		
$[CuPc]^{2-}$	$^2B_{1g}$	1.58	2.90	1.15(L-$2e_g\rightarrow$L-b_{1u})		
$[CuPc]^{3-}$	^2E_g	1.55	2.79	1.01(L-$2e_g\rightarrow$L-b_{1u})		
ZnPc	$^1A_{1g}$	1.44 (1.82)	2.85 (3.57)			
$[ZnPc]^+$	$^2A_{1u}$	1.44 (2.25)	2.69 (3.27)	1.29(L-$1e_g\rightarrow$L-a_{1u})		
$[ZnPc]^-$	^2E_g	1.49 (1.95)	2.90 (3.84)	1.29(1.31)(L-$2e_g\rightarrow$L-b_{1u})		
$[ZnPc]^{2-}$	$^1A_{1g}$	1.57 (2.38)	2.83 (3.70)	1.15(L-$2e_g\rightarrow$L-b_{1u})		
$[ZnPc]^{3-}$	^2E_g	1.52 (2.18)	2.73 (3.65)	1.02(1.13)(L-$2e_g\rightarrow$L-b_{1u})		
MgPc	$^1A_{1g}$	1.40 (1.85)	2.83 (3.65)			
$[MgPc]^+$	$^2A_{1u}$	1.42	2.67	1.34(L-$1e_g\rightarrow$L-a_{1u})		
$[MgPc]^-$	^2E_g	1.47 (1.94)	2.85 (3.65)	1.31(1.29)(L-$2e_g\rightarrow$L-b_{1u})		
$[MgPc]^{2-}$	$^1A_{1g}$	1.54 (2.38)	2.74 (3.70)	1.17(L-$2e_g\rightarrow$L-b_{1u})		
$[MgPc]^{3-}$	^2E_g	1.49 (2.10)	2.63 (3.66)	1.05(1.11)(L-$2e_g\rightarrow$L-b_{1u})		

[a]Evaluated with Slater transition state method.
[b]Reference 18.
[c]The notation L→M refers to ligand (Pc) to metal charge transfer transition, and vice versa for M→L.
[d]Reference 47.

Some of the present systems (e.g., FePc, CoPc) have more complex electronic structure, where metal $3d$ levels lie between the Pc HOMO and LUMO. For such systems, there are extra absorption features that may arise from charge transfer transitions.[17,18,21] The assignment of these bands is thus somewhat ambiguous. Calculations for several electronic transitions in the various MPc species and their ions may help resolve some of these questions, especially the sensitivity of the transition energies to the nature of the metal.

The spectra of MPc contain two principal visible region features labeled as Q and Soret bands, which are attributed to the allowed $a_{1u}\rightarrow 2e_g$ and $a_{2u}\rightarrow 2e_g$ transitions, respectively. The calculated energies for various transitions are collected in Table X, together with available experimental data[18,47] (most of the observed spectra were measured in solution).

The $a_{1u}\rightarrow 2e_g$ transition, Q band: Compared with the experimental data, the calculated transition energies for the Q band are generally too small by 0.2–0.6 eV. The calculations have not taken the solution environment into account, which may affect the electronic transitions.[18] In spite of some quantitative discrepancies with the measurements, good qualitative agreement is found between the calculations and experiment. The results show the following features for the Q band. (1) The transition energy increases slightly from $[MPc]^{x-}$ to $[MPc]^{(x+1)-}$ due to the differential spin-pairing energy. (2) The excitation energies are insensitive to ionization to $[MPc]^+$. (3) The nature of M has some influence on the transition energy, which decreases steadily as M progresses from Fe to Zn. (4) The transition in the $[MPc]^{x-}$ ion with a $(2e_g)^2$ configuration occurs at notably higher energy than that in other $[MPc]^{x-}$ ions. This enlargement may be ascribed to the Jahn–Teller distortion effect (see Sec. III B 7); the calculated results exhibit less pronounced Jahn–Teller effects than do the experimental data. (5) The HOMO(a_{1u})→LUMO($2e_g$) excitation pattern is different from the HOMO–LUMO energy differences in Fig. 2.

The $a_{2u}\rightarrow 2e_g$ transition, Soret band: As in the case of the Q band, the calculated transition energies for the Soret band are qualitatively consistent with the available experimental data, albeit underestimated by 0.4–0.8 eV. The values diminish slowly in progressing across the periodic table from Fe to Zn. Unlike the Q-band case, the Soret transition in $[MPc]^+$ occurs at lower energy than in MPc. Within the

TABLE XI. Calculated properties[a] of MPc with two axial ligands.

	$MPc(CO)_2$					
	M=Fe	M=Co	M=Ni	M=Cu	M=Zn	M=Mg
R_{C-O}[b]	1.147	1.144	1.136	1.139	1.137	1.136
R_{M-CO}	1.83	2.05	3.15	2.84	2.62	2.53
R_{M-N}	1.97	1.97	1.92	1.98	2.02	2.02
	(1.92)	(1.92)	(1.92)	(1.98)	(2.01)	(2.01)
E_{bind}[MPc–$(CO)_2$][c]	−2.01	−0.57	−0.11	−0.09	−0.01	−0.19
1st IP (a_{1u})	6.50	6.48	6.45	6.44	6.42	6.39
	(6.46)	(6.47)	(6.56)	(6.51)	(6.56)	(6.52)
		6.39[d]				
Q_M	0.36	0.28	0.47	0.53	0.49	0.72
	(0.71)	(0.59)	(0.50)	(0.65)	(0.64)	(0.87)
$a_{1u}\rightarrow 2e_g$	1.52	1.50	1.50	1.47	1.44	1.39
	(1.64)	(1.56)	(1.50)	(1.46)	(1.44)	(1.40)
$a_{2u}\rightarrow 2e_g$	2.83	2.87	2.99	2.90	2.82	2.80
	(3.13)	(3.10)	(3.00)	(2.92)	(2.85)	(2.83)

[a]Bond length R in Å; binding energy E_{bind}, ionization potential IP and transition energy in eV; the values in parentheses are those obtained for MPc.
[b]R_{C-O}= 1.139 Å in isolated CO.
[c]Binding energy between MPc and two CO's.
[d]When the electron is ionized from the a_{1g} orbital (see Fig. 4).

anion series, there is a mild lowering of the transition energy from MPc to $[MPc]^{3-}$. The Soret transition is also unaffected by the JT effect.

The $1e_g\rightarrow a_{1u}$ and $2e_g\rightarrow b_{1u}$ transitions: The a_{1u} orbital is singly occupied in $[MPc]^{+}$. The presence of an electron hole in a_{1u} permits allowed transition from $1e_g$. In the spectra of $[ZnPc]^{+}$ and $[MgPc]^{+}$, a band observed near 12 000 cm^{-1} (1.49 eV) was thought to perhaps arise from a $1e_g\rightarrow a_{1u}$ transition.[18] The calculated $1e_g\rightarrow a_{1u}$ transition energies are 1.29 and 1.34 eV, for these two species, respectively. As the calculated values seem to represent underestimates of some 0.2 eV, this finding supports the proposed assignment of the transition. Upon addition of electrons to form the $[MPc]^{x-}$ anions, transitions from $2e_g(\pi^*)$ to $b_{1u}(\pi^*)$ may be expected. The transition energy exhibits variation with M and x, increasing in the sequence from Fe to Ni, and diminishing from $x=1$ to $x=3$. Beyond Ni, however, the transition energy is static from one metal to the next.

Charge transfer (CT) transitions: We have calculated a few allowed CT transitions in FePc, CoPc, NiPc, and CuPc. These systems possess empty or partially filled $3d$-like MOs into which a CT transition could occur from the Pc a_{1u} or a_{2u}. The $a_{1u}\rightarrow 1e_g$ transition in FePc and CoPc occurs at very low energy, since the a_{1u} and $1e_g$ levels in the two systems are rather close. Another ligand (Pc) to metal (L→M) CT transition involving $a_{2u}\rightarrow 1e_g$ can occur between the Q and Soret bands. The metal to ligand (M→L) CT transition energy from $1e_g\rightarrow b_{1u}$ is high and increases from M=Fe to Co. In NiPc, the $3d$-like b_{1g} orbital lies below the $2e_g$. However, the transition $a_{1u}\rightarrow b_{1g}$ actually occurs at significantly higher energy than the $a_{1u}\rightarrow 2e_g$ transition. The M→L CT transition energies from $a_{1g}\rightarrow b_{1u}$ in $[FePc]^{x-}$ were also evaluated. They decrease strongly from $x=1$ to $x=4$. Some CT transitions are shown to have similar transition energies to the Q or Soret band, and they may be obscured by the main bands in the spectra.

F. Effect of strong-field axial ligands

Experiments have shown that when placed in a strongly coordinating solvent, $(solvent)_2FePc$ is low spin, diamagnetic.[22,24] While the calculations indicate a ^2E_g ground state for free CoPc, association with axial ligands leads to a $^2A_{1g}$ ground state.[25] These discrepancies suggest that interaction with strong-field axial ligands may affect the electronic structure of FePc and CoPc. To examine the effects of axial ligands, two CO molecules were placed above and below the MPc plane, with the C end pointing directly toward the M atom. The calculated properties of the resulting $MPc(CO)_2$ are reported in Table XI and the changes of the orbital levels are illustrated in Fig. 4.

Upon binding to the metal atom, the CO bond length undergoes a change of variable magnitude. This bond length is 1.139 Å in the isolated molecule. Examination of the first row of Table XI suggests that this bond stretches when bonded to Fe and Co, but that small contractions occur when bonded to the other four metals. The binding energy between FePc and a pair of CO molecules is quite large, 2 eV. Much smaller but still appreciable at 0.6 eV is the same quantity for $CoPc(CO)_2$, whereas the binding energy of the other MPcs listed in Table XI is much smaller, 0.1 eV and less. The M···C distances correlate with the energetics to some degree, with R(Fe···C) the shortest, followed by R(Co···C). Comparison of the M···N distances within the MPc complex (in parentheses) with the modified distance in $MPc(CO)_2$ reveals this bond length undergoes an appreciable lengthening, of some 0.05 Å, in only the Fe and Co complexes. Other factors support the notion that Fe and Co are most affected by the axial ligands. The metal atomic charges Q_M, are made more positive by the CO ligands for all metals. Whereas this charge increase is roughly 0.1 for Ni through Mg, it is 3 to 4 times higher for Co and Fe. The latter two metals also are connected with substantial enlargements of the excitation energies to the $2e_g$ orbital from both a_{1u} and

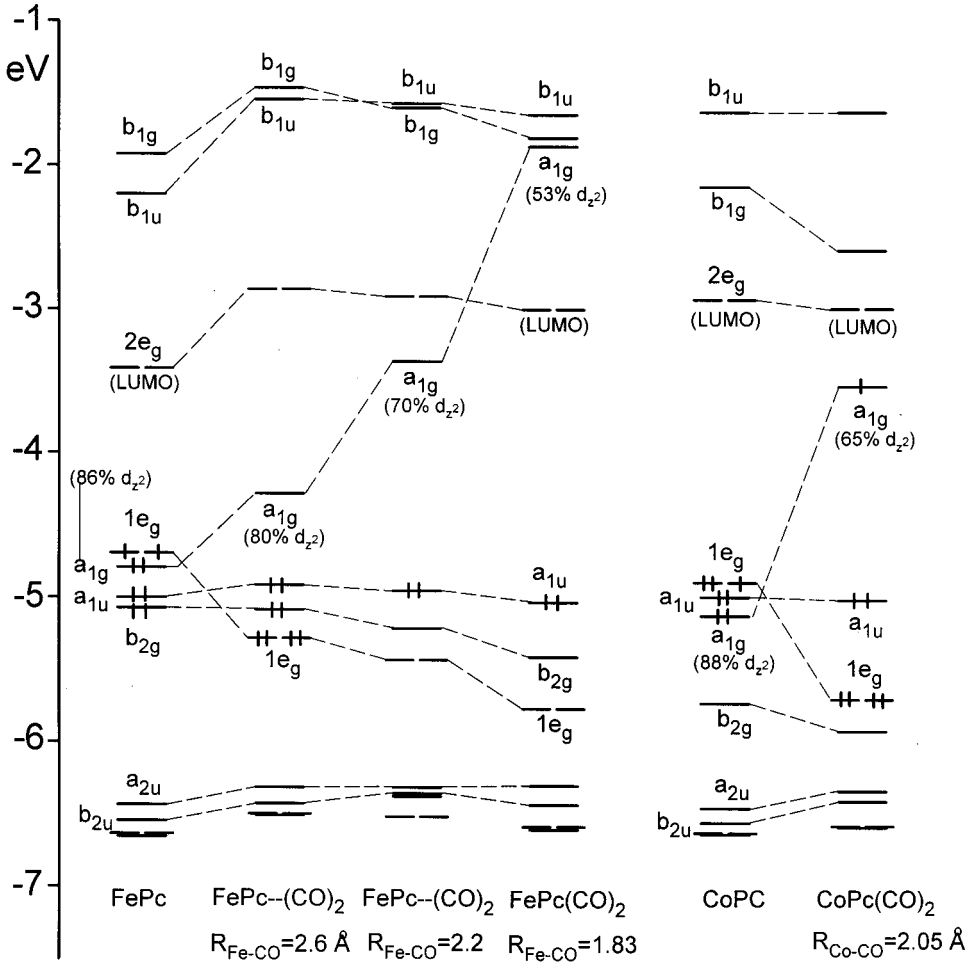

FIG. 4. Orbital energy level diagrams of FePc and CoPc when complexed with a pair of CO ligands.

a_{2u}. Curiously, this pattern of larger changes for Fe and Co reverses in the case of the ionization potentials, where it is the Ni, Cu, Zn, Mg series that undergoes larger changes upon complexation with the axial ligands.

The most striking feature of Fig. 4 is the very strong sensitivity of the energy of the $a_{1g}(\mathrm{M}-d_{z2})$ orbital in FePc and CoPc to the proximity of the CO ligands. This orbital is destabilized by nearly 3 eV in $\mathrm{FePc(CO)_2}$ when these ligands are brought in to their equilibrium distance of 1.83 Å. At the same time a number of the other orbitals, most notably $1e_g(\mathrm{M}-d_\pi)$ and $b_{2g}(\mathrm{M}-d_{xy})$ are pushed down. These reorderings result in a shift of electrons such that the HOMOs in $\mathrm{FePc(CO)_2}$ and $\mathrm{CoPc(CO)_2}$ become, respectively $(a_{1u})^2$ and $(a_{1g})^1$, yielding $^1A_{1g}$ and $^2A_{1g}$ ground states. Because the a_{1g} level in $\mathrm{CoPc(CO)_2}$ is raised, the IPs from a_{1g} and a_{1u} are now nearly equal.

IV. CONCLUSIONS

This systematic study of electronic structure and bonding in a series of metal phthalocyanines MPc (M=Fe, Co, Ni, Cu, Zn, Mg) and some of their ions has focused on a number of properties of the systems. Geometry optimizations suggest that these structures belong essentially to the D_{4h} point group, with perhaps very small deformations therefrom. The M–N distances are shortest for the Fe, Co, and Ni complexes with Pc. Ionization has little influence upon the internal geometry of the Pc ring.

The Pc MOs are interspersed with the *d* orbitals of the central metal atom. The energies of the M orbitals diminish as one progresses across the periodic table from M=Fe to Zn, whereas the Pc MOs are rather constant in energy. In FePc and CoPc, several $3d$-like orbitals are located near the Pc HOMO a_{1u}, such that the HOMO is of $\mathrm{M}-3d_\pi$ type. The calculation supports the assignment of free FePc as $^3A_{2g}$, which arises from the configuration $(d_{z2})^2(d_{xy})^2(d_{xz})^1(d_{yz})^1$. However, the energies of the $^3B_{2g}$ and ^3E_g states, related to $^3A_{2g}$ by displacements of electrons into d_π from d_{z2} and d_{xy}, are very close to that of $^3A_{2g}$. CoPc's electronic structure is very similar to that of FePc, with the addition of an electron into the $1e_g$ level, and with a number of states lying very close in energy to the ground state. In either case, oxidation removes an electron from the Pc a_{1u} orbital, whereas reduction places an electron into the partially filled $1e_g$. The situation is somewhat different in the other MPc's, as the metal *d* orbitals sink below the Pc a_{1u}, the energy of which is quite insensitive to changes in the metal, making the latter the HOMO of the entire system. Ionization of all MPc's occurs from the Pc a_{1u} orbital, so that the first ionization potentials are all quite similar, and

independent of the metal. Whereas the first reduction in FePc and CoPc occurs at the metal, it is the Pc ring that is reduced upon addition of electrons to the other systems. FePc, NiPc, and CuPc have a HOMO–LUMO separation in the neighborhood of 1.4 eV; those of ZnPc and CoPc are somewhat larger, nearly 2 eV.

The effective charge on the metal atoms is found to lie in the 0.5–0.7 range for the tMPc's, with the precise value not necessarily reflecting the electronegativity of each. There is very little variation in atomic charges within the Pc ring from one metal to the next. The metal atoms are strongly bound to the ring in these complexes. The binding energies lie in the 6–10 eV range, with a tendency for larger values on the left side of the periodic row. All MPc's have a strong attraction for an electron, particularly FePc and CoPc. The energy required to extract an electron is nearly constant for all MPc's at approximately 6.5 eV; this electron is removed from the Pc HOMO in each case. The nature of M has some influence on the transition energies of the *Q* and Soret bands, which decrease steadily as M progresses from Fe to Zn. Electronic structures are subject to the influence of strong-field axial ligands, which bind particularly strongly in the case of $FePc(CO)_2$. The energy of the iron's d_{z2} orbital is destabilized a great deal by the presence of the CO ligands, while some of the other *d* orbitals are lowered in energy. The resulting reordering shifts electrons and changes the ground electronic state of $FePc(CO)_2$ as well as $CoPc(CO)_2$.

ACKNOWLEDGMENTS

This work was supported by Grant No. DAAD19-99-1-0206 from the Army Research Office. We are grateful to Professor Samson Jenekhe for helpful discussions.

[1] A. B. P. Lever, M. R. Hempstead, C. C. Leznoff, W. Lin, M. Melnik, W. A. Nevin, and P. Seymour, Pure Appl. Chem. **58**, 1467 (1986).
[2] For a review on phthalocyanine applications, see E. Orti and J. L. Brédas, J. Am. Chem. Soc. **114**, 8669 (1992), and references therein.
[3] H. Ali and J. E. van Lier, Chem. Rev. **99**, 2379 (1999).
[4] J. M. Robertson, J. Chem. Soc. 195 (1936).
[5] A. Henriksson and M. Sundbom, Theor. Chim. Acta **27**, 213 (1972); A. Henriksson, B. Roos, and M. Sundbom, *ibid.* **27**, 303 (1972).
[6] R. E. Linder, J. R. Rowland, and N. S. Hush, Mol. Phys. **21**, 417 (1971).
[7] S. G. Mathur and J. Singh, Int. J. Quantum Chem. **6**, 57 (1972).
[8] A. J. McHugh, M. Gouterman, and J. Weiss, Theor. Chim. Acta **24**, 346 (1972).
[9] D. W. Clack and M. Monshi, Inorg. Chim. Acta **22**, 261 (1977).
[10] L. K. Lee, N. H. Sabelli, and P. R. Lebreton, J. Phys. Chem. **86**, 3926 (1982).
[11] F. W. Kutzler and D. E. Ellis, J. Chem. Phys. **84**, 1033 (1986).
[12] E. Orti and J. L. Brédas, J. Chem. Phys. **89**, 1009 (1988).
[13] A. Ghosh, P. G. Gassman, and J. Almlöf, J. Am. Chem. Soc. **116**, 1932 (1994).
[14] P. N. Day, Z. Wang, and R. Pachter, J. Mol. Struct.: THEOCHEM **455**, 33 (1998).
[15] D. P. Piet, D. Danovich, H. Zuilhof, and E. J. R. Sudhölter, J. Chem. Soc., Perkin Trans. 2 1653 (1999).
[16] B. Szczepaniak and P. Bragiel, Vacuum **46**, 465 (1995).
[17] A. B. P. Lever, S. R. Pickens, P. C. Minor, S. Licoccia, B. S. Ramaswamy, and K. Magnell, J. Am. Chem. Soc. **103**, 6800 (1981).
[18] P. C. Minor, M. Gouterman, and A. B. P. Lever, Inorg. Chem. **24**, 1894 (1985).
[19] M.-S. Liao and S. Scheiner (unpublished).
[20] B. G. Johnson, P. M. W. Gill, and J. A. Pople, J. Chem. Phys. **98**, 5612 (1993).
[21] D. W. Clack and J. R. Yandle, Inorg. Chem. **11**, 1738 (1972).
[22] A. B. P. Lever and J. P. Wilshire, Inorg. Chem. **17**, 1145 (1978).
[23] C. G. Barraclough, R. L. Martin, S. Mitra, and R. C. Sherwood, J. Chem. Phys. **53**, 1643 (1970).
[24] M. J. Stillman and A. J. Thomson, J. Chem. Soc., Faraday Trans. 2 **70**, 790 (1974).
[25] F. Cariati, D. Galizzioli, F. Morazzoni, and C. Busetto, J. Chem. Soc. Dalton Trans. 556 (1975).
[26] (a) N. Toshima and T. Tominage, Bull. Chem. Soc. Jpn. **69**, 2111 (1996); (b) N. Toshima, T. Tominage, and S. Kawamura, *ibid.* **69**, 245 (1996); (c) N. Toshima, S. Kawamura, and T. Tominage, Chem. Lett. 1299 (1993).
[27] A. L. Allred, J. Inorg. Nucl. Chem. **17**, 215 (1961).
[28] H. Ozaki and Y. Harada, J. Chem. Phys. **92**, 3184 (1990).
[29] ADF program package, version 2.0.1: E. J. Baerends, D. E. Ellis, and P. Ros, Chem. Phys. **2**, 41 (1973); G. te Velde and E. J. Baerends, J. Comput. Phys. **99**, 84 (1992).
[30] T. Ziegler, V. Tschinke, E. J. Baerends, J. G. Snijders, and W. Ravenek, J. Phys. Chem. **93**, 3050 (1989).
[31] T. Ziegler and A. Rauk, Theor. Chim. Acta **46**, 1 (1977).
[32] S. H. Vosko, L. Wilk, and M. Nusair, Can. J. Phys. **58**, 1200 (1980).
[33] A. D. Becke, Phys. Rev. A **38**, 3098 (1988).
[34] J. P. Perdew and Y. Wang, Phys. Rev. B **33**, 8800 (1986).
[35] J. L. Kahl, L. R. Faulkner, K. Dwarakanath, and H. Tachikawa, J. Am. Chem. Soc. **108**, 5434 (1986).
[36] J. F. Kirner, W. Dow, and W. R. Scheidt, Inorg. Chem. **15**, 1685 (1976).
[37] G. A. Williams, B. N. Figgis, R. Mason, S. A. Mason, and P. E. Fielding, J. Chem. Soc. Dalton Trans. 1688 (1980).
[38] J. M. Robertson and I. Woodward, J. Chem. Soc. 219 (1937).
[39] C. J. Brown, J. Chem. Soc. A 2488 (1968).
[40] W. R. Scheidt and W. Dow, J. Am. Chem. Soc. **99**, 1101 (1977).
[41] B. Assmann, G. Ostendorp, G. Lehmann, and H. Homborg, Z. Anorg, Allg. Chem. **622**, 1085 (1996).
[42] C.-Y. Ruan, V. Mastryukov, and M. Fink, J. Chem. Phys. **111**, 3035 (1999).
[43] J. C. Slater, *Quantum Theory of Molecules and Solids* (McGraw-Hill, New York, 1974), Vol. 4.
[44] J. Berkowitz, J. Chem. Phys. **70**, 2819 (1979).
[45] J.-H. Fuhrhop, K. M. Kadish, and D. G. Davis, J. Am. Chem. Soc. **95**, 5140 (1973).
[46] A. Wolberg and J. Manassen, J. Am. Chem. Soc. **92**, 2982 (1970).
[47] B. H. Schechtman and W. E. Spicer, J. Mol. Spectrosc. **33**, 28 (1970).